Hindawi
Advances in Civil Engineering
Volume 2020, Article ID 8834773, 16 pages
https://doi.org/10.1155/2020/8834773

Research Article

Experimental Behavior of the Curved Continuous Twin I-Girder Composite Bridge with a Precast Concrete Slab Subjected to Bending, Shear, and Torsion

Chuandong Shen,[1] **Yifan Song**,[1] **Lei Yan**,[1] **Yuan Li**,[1] **Xueli Wang**,[2] **and Shuanhai He**[1]

[1]*School of Highway, Chang'An University, Xi'an 710064, China*
[2]*Shanxi Expressway Construction Group Company, Xi'an 710065, China*

Correspondence should be addressed to Chuandong Shen; shenchuandong1991@126.com and Yifan Song; syf@chd.edu.cn

Received 15 July 2020; Revised 13 October 2020; Accepted 22 October 2020; Published 16 November 2020

Academic Editor: John Mander

In order to investigate the mechanical behavior, ultimate load carrying capacity, and failure mode of the intact curved continuous twin I-girder composite bridge (TGCB) with a precast concrete slab, one curved continuous composite bridge model with a scale ratio of 1 : 5 of a prototype bridge was designed and manufactured considering the influence of the construction sequence. Four symmetric point loads' test was carried out. In this paper, load-deflection relationship and strain development of steel girders, concrete slab, and reinforcement at key sections were tested and analyzed. Failure mode, crack development, and major crack width at the top surface of the concrete slab in the hogging moment region were also reported. The experimental results demonstrated that the load capacity under the initial cracking level, cracking level with the width of 0.2 mm, and steel girder yielding state is about 1.7, 5.0, and 6.3 times of the design load, respectively. Due to the influence of curvature, the stiffness of the external girder is less than that of the internal girder. However, the ultimate bearing capacity is basically the same, approximately 13.6 times of the design load. During the loading process, plastic hinge was first observed at the intermediate support section as a result of the hogging moment which should be emphasized in design. The local buckling took place after yielding, indicating a class 2 section according to Eurocode 4. In addition, the TGCB had good ductility since the displacement ductility coefficients of the external and internal girders were 4.40 and 4.06, respectively.

1. Introduction

Composite bridges of the precast concrete slab on the twin I-girder are a very attractive form for short and medium span bridges because the system can ensure the quality of the concrete slab and reduce construction time and costs [1, 2]. The twin I-steel girder is connected with the precast concrete slab by studs (shown as Figure 1). This type of superstructure may be regarded as a typical candidate for ABC techniques. In addition, the advantages also included its practicality, economy, and simplicity in construction compared with multigirder steel bridges and high span-to-depth ratio, ability to adapt their geometry to design constraints, and the possibility of reusing some of the materials in the structure compared with concrete bridges [3–6]. With the above advantages, twin I-girder steel-concrete composite bridge has been used extensively in Japan, the United States, and throughout the world [7, 8].

Ultimate load carrying capacity is an important index to evaluate the serviceability margin under service load and capacity of overload [9, 10]. However, experiment is the most credible and effective means to obtain the ultimate load carrying capacity and failure mode, as well as to evaluate the mechanical performance [11–14]. A lot of experimental works have been conducted to study the ultimate strength and performance of the composite girder [15–18]. From previous experimental studies, it could be found that the objects of tests mainly included steel-concrete composite girders and steel-concrete composite bridges. A large number of experimental studies were carried out on simply

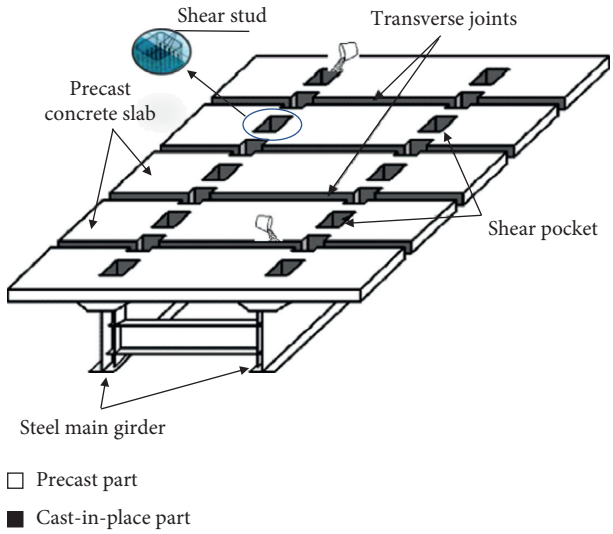

Figure 1: Twin I-girder composite bridge with the precast concrete slab.

supported or continuous composite I-girder specimens [16–25]. Compared with the intact structure, the specimen has several advantages when used as an experiment objective, such as easy fabrication, small dimensions, and low cost. So, it is more possible to carry out comparative experiments on different parameters. In addition, constraints and loading are easy to implement in the laboratory.

Although it has so many advantages, few of these experiments could consider the influence of transverse beams on the mechanical behavior as Kennedy and Grace [26] and Soliman and Kennedy [27] indicated that transverse beams had a significant effect on the load carrying capacity of a composite bridge. However, intact steel-concrete composite bridge models (including full-scale models and scale models) could avoid the shortage of composite girder specimens. Thus, it is more meaningful to conduct experiments on intact bridge models compared to specimens. Unfortunately, there were fairly limited experimental studies on the twin I-girder steel-concrete composite bridge model since it was constrained by production cost, test scale, or other condition [10, 28–30]. In addition, it is worth mentioning that the influence of construction initial stress is not considered in both composite girder and composite bridge models, which has been proved having an impact on the load carrying capacity of CFST members by Han and Yao [31]. As we know, twin I-girder steel-concrete composite bridge is also a typical self-erecting system bridge. The steel girders play a role of support before the formation of the composite section. Because bare steel girders bear the weight of themselves and the concrete slab, they inevitably produce the initial construction stress before the formation of the composite section. Therefore, it is necessary to consider the influence of initial stress in the ultimate load carrying capacity of the composite bridge when conducting bridge model experiments. On the contrary, fewer experimental studies were conducted to investigate the mechanical performance of the curved composite bridge compared to the straight composite bridge. Nowadays, the number of existing or under-construction curved composite bridges is increasing gradually in China. Therefore, it is of great significance for the development of engineering practice to carry out the whole process loading test research of the intact curved continuous composite bridge.

In order to study the mechanical behavior and the ultimate load carrying capacity of the curved twin I-girder steel-concrete composite bridge, in this paper, based on the similarity theory, a two-span curved continuous composite bridge model with a scale ratio of 1 : 5 of the prototype bridge was designed and manufactured. The prototype bridge was a 2-span continuous composite bridge with spans of 35 m for a total span of 70 m with a precast reinforced concrete deck. In order to obtain the completed state equivalent to the stress of the prototype bridge, the 1/5-scale bridge model considered the influence of the construction initial stress by simulating the construction sequence of the prototype bridge. And the self-weight was compensated during the construction process. A comprehensive static test was cautiously carried out on the bridge model. Load-deflection relationship and strain development of steel girders, concrete slab, and reinforcement at key sections were measured and analyzed. Moreover, crack development, major crack width, ultimate strength, and failure modes were evaluated. This paper introduced the experimental program and the most relevant results in detail. These results will be used to verify the numerical model, and the influence of several key parameters will be further studied.

2. Experimental Works

2.1. Model Design. A prototype bridge (Figure 2), located in Shanxi province, China, was a curved continuous twin I-girder composite bridge with two spans (2×35 m) designed by current China highway standard specifications [32–34]. The radius of curvature of the centerline was 460 m. The height of the composite girder was 2.2 m. The width of the top concrete slab was 12.75 m. The width of the cantilever part of the top concrete slab was 3.025 m. The thickness of this cantilever part varied from 0.22 m at the free end to 0.4 m at the intersection over the steel web.

Based on the similarity principle, an intact 1/5-scale curved bridge model (bridge model for short hereafter in this paper) was designed, manufactured, and loaded to failure. The bridge model was also designed as fully bonded as the prototype bridge. The typical geometry of the bridge model is shown in Figure 3. The detail dimensions of all steel plates are summarized in Table 1. The two-span model was 14,000 mm long and continuously supported on each span of 6814 mm and consisted of two main steel I-girders, twenty precast concrete slabs, and eleven crossbeams. The radius of curvature of the centerline was 92 m after scaling the radius of the prototype bridge ($R = 460$ m). The height of the main steel girders was 360 mm. The space between two main steel girders was 1340 mm. The space between two crossbeams was 1400 mm. The width of the precast slab was 2550 mm. The thickness of the concrete slab was 44 mm~80 mm. Each precast slab had four shear pockets for stud shear connectors. The bond between steel beams and the concrete slab

Figure 2: Prototype bridge.

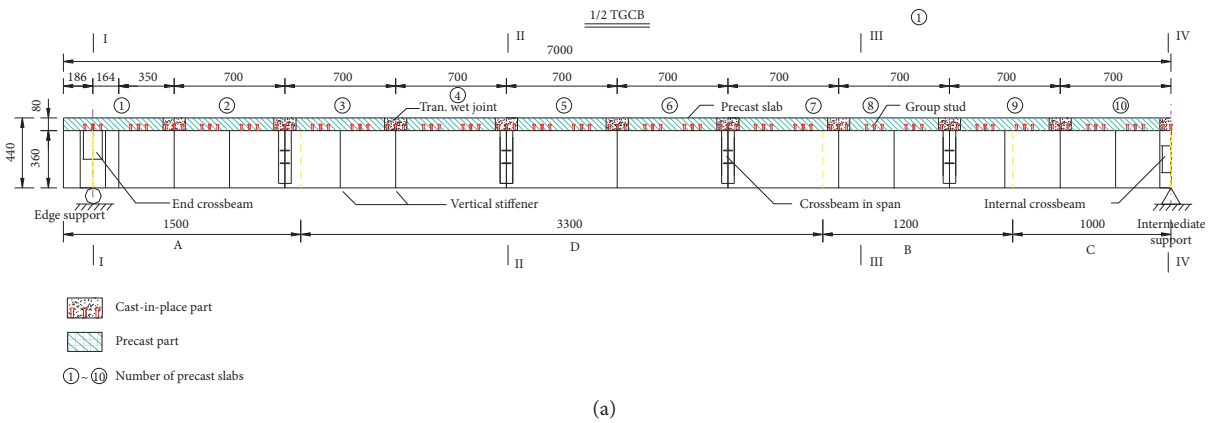

(a)

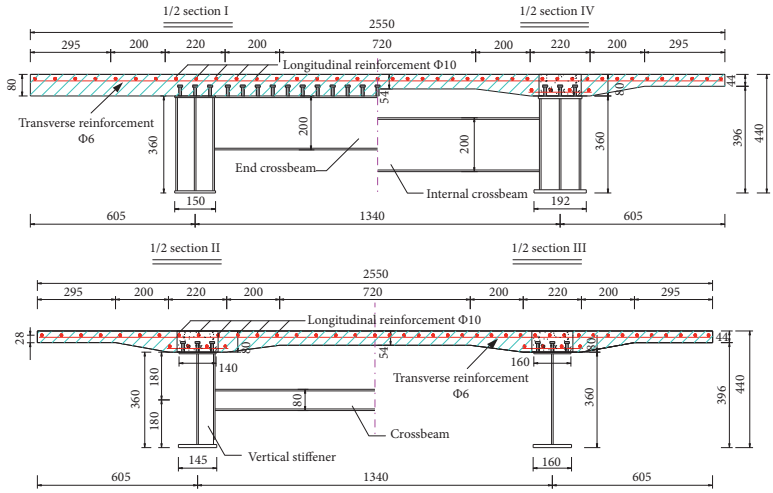

(b)

Figure 3: Continued.

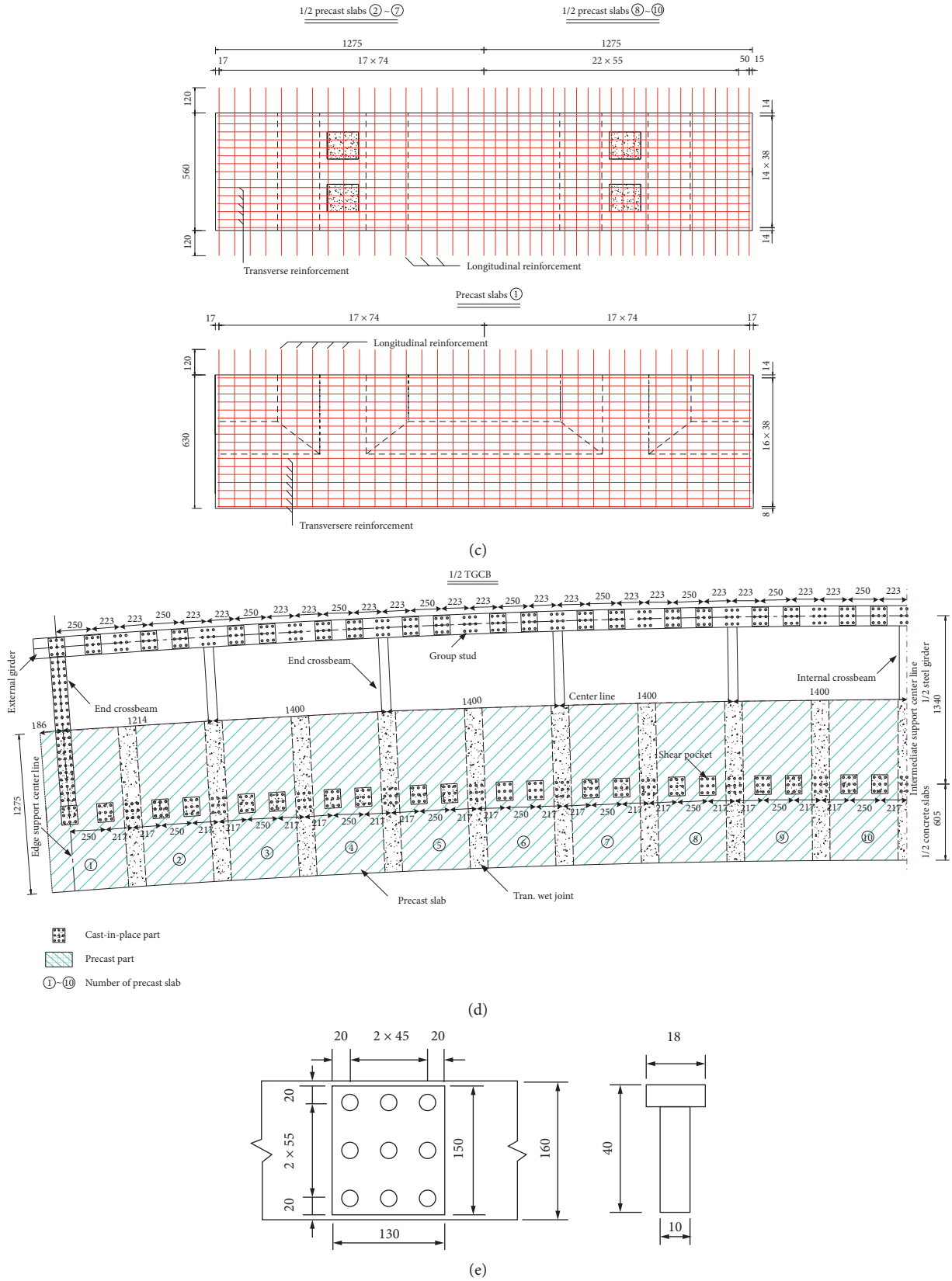

Figure 3: Typical geometry of the bridge model (unit: mm). (a) Vertical view (1/2 span). (b) Cross section. (c) Layout of reinforcement. (d) Top view (1/2 span). (e) Arrangement of the group studs.

Table 1: The detail dimensions of all steel plates (unit: mm).

Component	Section position	Steel plates' dimensions				
		Web	Top flange		Bottom flange	
		Thickness	Width	Thickness	Width	Thickness
Main girder	*A*	6	150	6	150	8
	B	6	160	8	160	8
	C	6	160	10	192	12
	D	6	140	6	145	12
Crossbeam	End crossbeam	6	120	6	120	6
	Internal crossbeam	6	120	6	120	6
	Crossbeam in span	6	60	6	60	6

was achieved by means of group studs. The diameter and height of the stud were 10 mm and 40 mm, respectively. The arrangement of the group studs can be seen in Figure 3(e).

2.2. Mechanical Properties of Materials. A summary of the properties of the materials used is shown in Tables 2 and 3. C50 fine aggregate (less than 10 mm) concrete was used for the precast concrete slab. In order to minimize the effects due to initial drying shrinkage, expansive concrete was cast in the transverse wet joints between decks. Nonshrinkage mortar was cast as the filling material in the shear pockets to combine the shear connectors and the slab. The steel plate applied for the model was Q345b with a thickness of 6 mm, 8 mm, 10 mm, and 12 mm. Transverse reinforcement and longitudinal reinforcements are HRB400 with a diameter of 6 mm and 10 mm, respectively. The shear studs were made of MLA15. The elastic modulus of concrete was obtained from the compression tests of three 300 mm × 150 mm × 150 mm prismatic specimens, and the compressive strength was measured from the compression tests of three 150 mm × 150 mm×150 mm cube tests. Tension tests were carried out for three steel coupons to determine the elastic modulus and the tensile strength of steel.

2.3. Construction of the Model. In order to obtain the equivalent construction initial stress and completion state of the prototype bridge, gravity compensation of the steel girder and concrete slab was conducted, respectively, during bridge model construction. The method of gravity compensation was hanging standard-weight sandbags under the main girders. And we use 18 channels playing a role of hammock in which sandbags can be stacked in. Because the linear dimension scaled factor is 1/5, we compensated four times the weight of the steel girder and concrete slab, respectively. Construction sequence of the bridge model and prototype bridge is presented in Table 4. Moreover, it should be noted that enough space was reserved under sandbags and hammock to make them deflect with the model. And the test results also verified that the space is enough exactly.

2.4. Loading and Measurement Location. Figure 4 shows the overview of the test setup. The test was carried out in the mixing station, near the prototype bridge. Because of the restriction of loading conditions, we had to make a test setup. The self-developed test setup consisted of a ground anchor, six anchor rods, and two reaction crossbeams, as shown in Figure 4. The ground anchor is made of about 100 m^3 concrete. The diameter and length of the finished deformed bar used as an anchor rod were 32 mm and 7500 mm, respectively. Each reaction crossbeam was 3.2 m long and welded together by three 36b I-beams. The results of both calculation and experiment show that the deformation of the reaction crossbeam is negligible compared with that of the model during the loading.

The bridge model was loaded with four 1000 kN hydraulic jacks which were controlled by one intelligent tension control system. Each jack load was distributed by a 250 × 250 × 30 mm rubber bearing plate. The load value (P) of each jack was measured by a 200 t pressure sensor (HM2D6-200) under the jack. Four pressure sensors were connected with a data acquisition system (TDS-303) so as to ensure the synchronous loading. In this way, two concentrated forces were applied at each midspan nearby. The distance between the two jacks in the transverse direction was just equal to the space between two main steel girders. According to the calculation, the equivalent load of the design load was 30 kN at each jack.

The schematic of the loading setup and instrumentation is shown in Figure 5. The arrangement of strain gauges, deflection dial gauges, and slip dial gauges is demonstrated in Figure 5(a). Figure 5(b) shows the layout of strain gauges on the steel girder and concrete slab at section *A*. The layout of strain gauges on other sections is the same as that on section *A*.

2.5. Test Procedures. The test was carried out under a loading control process. Four concentrated loads were applied to the model at a constant rate in increments of 10 kN. After each increment, the load was maintained constant during recording of the strains and deflections. When the beam was close to its failure stage, the test load was applied slowly and continuously. The test ended after the test model failed.

3. Test Results and Discussion

3.1. Test Phenomenon and Failure Mode. The testing up-to-failure of the bridge model began by applying the load in increments. At the initial loading stage, the whole bridge

Table 2: Material properties of concrete.

Material	Elastic modulus (MPa)	Compressive strength (MPa (standard deviation))
C50 fine aggregate (less than 10 mm) concrete	3.68×10^4	52.2 (0.91)
Expansive concrete	3.64×10^4	54 (0.75)
Nonshrinkage mortar	3.68×10^4	58 (0.88)

Table 3: Material properties of steel.

Material	Thickness (diameter/mm)	Elastic modulus (MPa)	Yielding strength (MPa)	Ultimate tensile strength (MPa)
Steel plate	6	2.03×10^5	394	563
	8		387	568
	10		406	574
	12		395	556
Reinforcement	6	2.00×10^5	571	754
	10		492	673
Shear stud	40×100	1.90×10^5	397	453

Note. All the values in Tables 2 and 3 are average values obtained from laboratory tests. The standard deviation of some results is given in brackets.

Table 4: Construction sequence of the bridge model and prototype bridge.

Construction sequence	Prototype bridge	Bridge model
Step 1	Lifting the first span steel main girder (40 m)	Lifting the first span steel main girder (8 m) and hanging weight compensation sandbags
Step 2	Lifting the second span steel main girder (30 m) and welding two-span girder together	Lifting the second span steel main girder (6 m), hanging weight compensation sandbags, and welding two-span girder together
Step 3	Installing precast concrete slabs in sequence	Installing precast concrete slabs in sequence and hanging weight compensation sandbags
Step 4	Pouring concrete in the shear pocket and transverse joints	Pouring concrete in the shear pocket and transverse wet joints
Step 5	Completing the deck pavement	Loading pavement weight sandbags

Figure 4: Overview of the test setup.

model worked well without abnormal noise. The steel girders and concrete slab showed a good combination. When the loading reached about 50 kN (about 1.7 times of the design load (30 kN) and 0.12 Pu), the first crack appeared on the top surface of the concrete slab at the interaction between the precast concrete and the wet joint concrete over the intermediate support. With the load increased continuously, the cracks propagated. The first crack extended gradually from the outer flange of the concrete slab to the inner along the transverse direction of the bridge and became a major crack. When the load exceeded 80 kN (about 2.7 times of the design load and 0.2 Pu), the main crack developed through the entire concrete slab at the transverse direction, which caused the concrete of the intermediate support section out of work. When the load exceeded 180 kN (about 6 times of the design load and 0.44 Pu), a sound from the bridge model was heard. At that time, the adhesive force between the steel beam and the concrete slab started to break locally. Then, when the load reached 190 kN (about 6.3 times of the design load and about 0.5 Pu), the bottom flange yielded at outer intermediate support, which was the first time that the steel girder yielded. This marked that the bridge model entered into the elastic-plastic stage from the elastic stage. As the load increased continuously, the bottom flange of the internal steel girder at the intermediate support position and the bottom flange of the load section entered into the yielding state, successively. When the load increased to 390 kN (about 13 times of the design load and about 0.95 Pu), longitudinal reinforcement approached the yield strength in the hogging moment zone. Then, the full section near the intermediate support was close to the yield, which marked the plastic hinge formed, and the structural system changed. With the load increasing to 407 kN (about 13.6 times of the design load and the ultimate load Pu), the deflection at the load section increased rapidly, as well as the major crack at the intermediate support. At that time, a

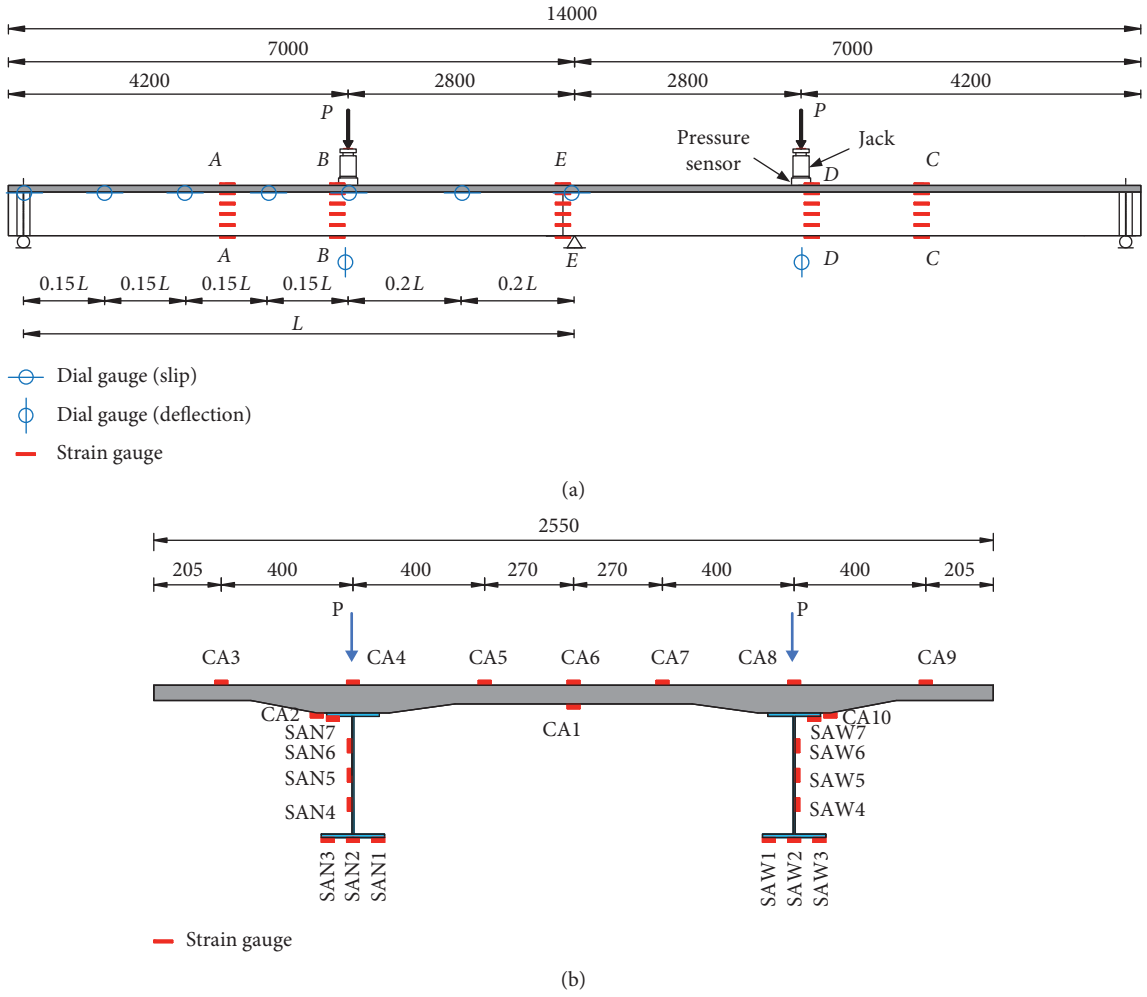

Figure 5: Schematic of the loading setup and instrumentation (unit: mm). (a) Vertical deflection and interface slip. (b) Layout of strain gauges on the steel girder and concrete slab (section *A*).

sound from the test model was heard. The concrete slabs were crushed along the transverse direction on the top surface of the concrete slab near the loading section. Then, with a rapid increase of deflection, the jack load gradually decreased. Due to the over large deflection, the loading was ended. However, the sandbags did not touch down ground during the test load.

Figure 6 shows the failure mode of the model under the ultimate state. Significant large deflection was recorded. The maximum crack width was up to 4 mm near the intermediate support section. The concrete slabs were crushed at the top of the concrete slab near the loading position. The webs of main girders were buckled locally at the loading position and intermediate support section, respectively. The whole bridge model presented an obvious "*W*" shape (Figure 6).

3.2. Main Test Results. Due to a large number of measuring points and the limitation of article length, this paper only presents and analyzes the main test results.

3.2.1. Load-Deflection Relationship. Figure 7 shows load-deflection curves at the loading position of the internal girder and external girder, respectively. According to the curves in Figure 7, the load-deflection curves of the internal and external girders have similar changing law, which could be divided into three stages: elastic stage (*O*-*A*), elastic-plastic stage (*A*-*B*), and failure stage (*B*-*C*). The main conclusions are as follows:

(1) Elastic stage: when the load was close to 50 kN (about 1.7 times of the design load and about 0.12 Pu), cracks appeared near the intermediate support section, and the slope of the load-deflection curve began to change slightly. Before reaching point "*A*," the bridge model was in the elastic state, where the deflection at the loading section increased linearly with the load. In this stage, the composite section worked well.

(2) Elastic-plastic stage: when the load reached 190 kN (about 6.3 times of the design load and about 0.5 Pu), close to point "*A*," the bottom flange of the steel girder section near the intermediate support began to yield. It can be seen from Figure 7 that the curve slope began to decrease. It indicated the structure stiffness reduction. In this process, when the load

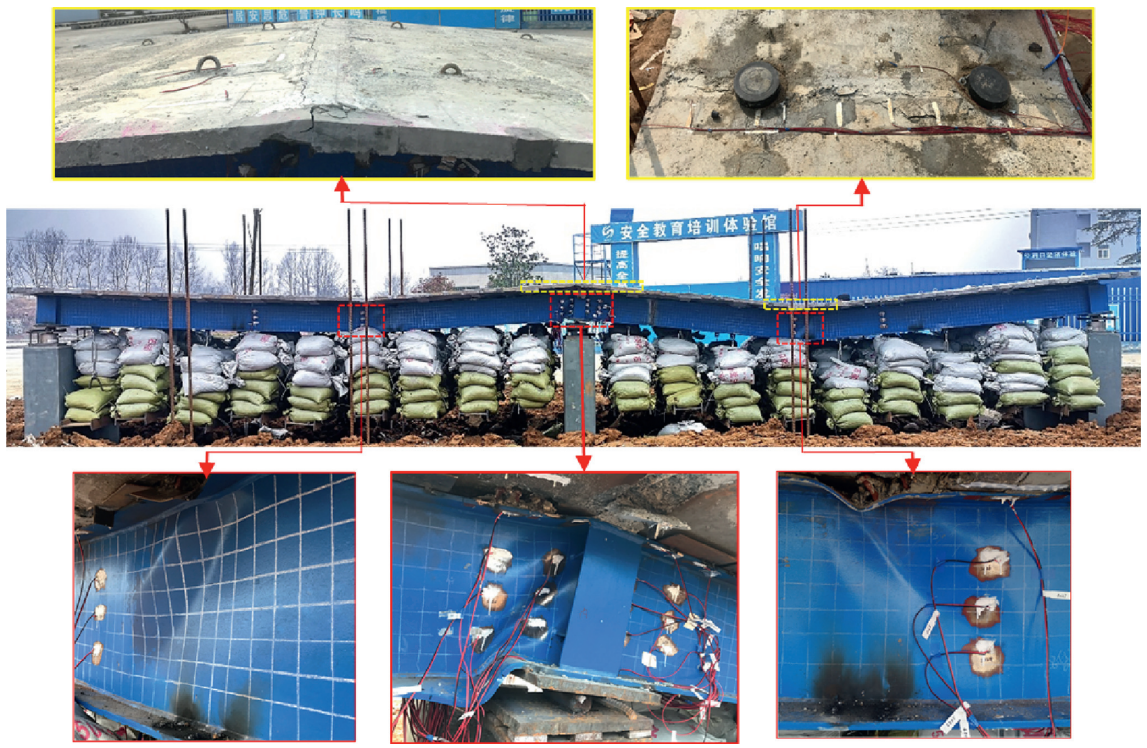

Figure 6: Failure mode of the model under the ultimate state (view of the internal girder).

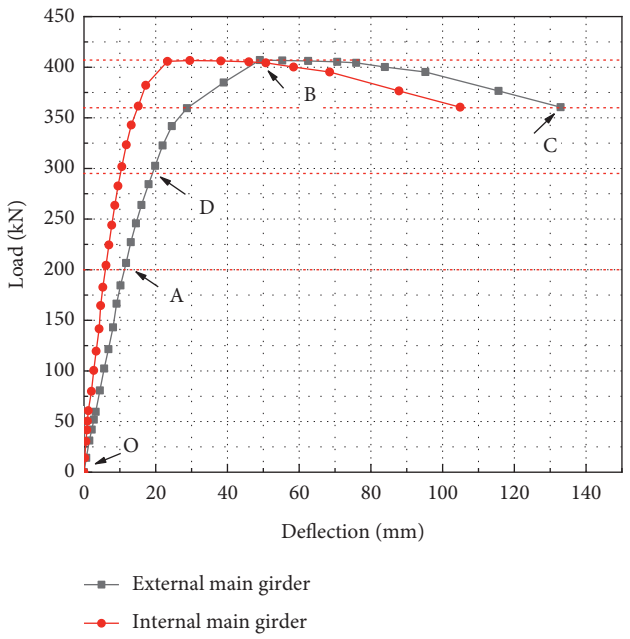

Figure 7: Load-deflection curves at the intermediate support section.

increased up to 300 kN (about 10 times of the design load and about 0.72 Pu), point "*D*," the bottom flange of the steel girder section near the loading position also began to yield, which made the load-deflection curve slope to continuously decrease. With the increase in deflection, the load and deflection showed an obvious nonlinear relationship.

(3) Failure stage: when the load reached 407 kN (about 13.6 times of the design load and the ultimate load Pu), as shown in Figure 7, point "*B*," the webs of both internal and external girders were buckled locally near the intermediate support section. A rotatable plastic hinge was formed at the intermediate support section. The change of the continuous beam structure system resulted in a redistribution of the internal force of the whole bridge model. Therefore, the deflection of the loaded section increased rapidly, a large area of the positive-moment steel beam yielded, and the concrete slab formed a crushing belt rapidly.

Define displacement ductility coefficient $\mu_\Delta = \delta_u/\delta_y$, where δ_u is the ultimate deflection corresponding to the ultimate load P_u and δ_y is the initial yield deflection corresponding to the yielding load P_y. Then, the displacement ductility coefficients of the internal and external girders were 4.06 and 4.40, respectively. In addition, after reaching the ultimate load carrying capacity, the deflection continuously increased with the decrease of load. It indicated that the composite girder had good ductility. And the ductility of the outer main girder was higher than that of the inner main girder.

It was also found from Figure 7 that there were slight differences between the stiffness of the internal girder and that of the external girder. The deflection of the external girder was faster than that of the external one. Taking the applied load of 300 kN (about 10 times of the design load and about 0.72 Pu) as an example, the corresponding deflection of the external steel girder was 19.84 mm, while the corresponding deflection of the internal steel girder was only

10.54 mm. There were two reasons for the difference of deflection between inside and outside of the model. On the one hand, it was the torsional effect of the curved bridge. On the other hand, the stiffness of the external and internal girders was different due to their different lengths. However, the length difference in this model was small, and the torsional effect was the main reason for this variation. Therefore, it is suggested that the influence of different curvatures on the inside and outside of the bridge should be considered even in the calculation of the deflection of the medium load.

3.2.2. Strain on the Steel Main Girders

(1) Strain on the Steel Main Girders in the Hogging Moment Region. Figures 8(a) and 8(b) show the load-strain curves (with tensile strain as positive) of strain measuring points on the external and internal steel main girder at the intermediate support section (section *E* in Figure 5(a)), respectively. In Figures 8(a) and 8(b), the intercept of the abscissa represents the initial construction strain caused by the self-gravity and concrete gravity of the steel girder as the support. The initial strain of the steel girder at the intermediate support section was about 400 $\mu\varepsilon$. The initial stress degree was defined as the ratio of the initial stress to the yield stress, so the corresponding initial stress degree was 0.2.

In the elastic stage, as the load increased, the strains developed linearly. Also, at the same loading level and strain measuring point location, the strain of the external steel main girder was larger than that of the internal steel main girder. It indicated that the stress of the external steel main girder of the curved bridge was more unfavorable than that of the internal steel main girder. According to the steel plate property test, the yielding strain was 1920 $\mu\varepsilon$. When the load increased up to 190 kN (about 6.3 times of the design load and about 0.5 Pu), the bottom flange of the steel girder near the intermediate support section yielded. This clearly indicated that the bridge model entered into the elastic-plastic stage.

In the elastic-plastic stage, with the increase of load, the bottom flange and web of the steel girder near the intermediate support section yielded gradually. Meanwhile, in this stage, there was a rapid change in some web strain sign near the bottom flange, in particular to SEW4 and SEN4. The compressive strain increased to a certain size and began to decrease. Finally, it transformed into tensile strain. It indicated the neutral axis of the composite section moved downward gradually. When approaching the ultimate load of 407 kN (about 13.6 times of the design load and Pu), the full section at the intermediate support position almost yielded. The entire bridge model entered into the failure stage. In the failure stage, the load-strain curves showed obvious yield steps, the maximum strain at the bottom flange was more than 10,000 $\mu\varepsilon$, and the plastic development in the negative moment zone had been very sufficient.

In accordance with Eurocode 4 [35], the sectional classes in hogging moment regions for the bridge model were regarded as class 2. That was to say, the composite section could form a plastic hinge and make full use of the mechanical properties of steel, but the rotation capacity is limited by the local buckling of the steel girder.

(2) Strain on the Steel Main Girders at the Positive Moment Region. Figure 9 shows the load-strain curve (with tensile strain as positive) of strain measuring points on the external and internal steel main girder at the loading section (section *B* in Figure 5(a)). It is clear from Figure 9 that the initial strain of the steel girder of the loading section is about 220 $\mu\varepsilon$. So, the corresponding initial stress degree is 0.12. When the load increased up to 240 kN (about 8 times of the design load and about 0.6 Pu), the bottom flange of the steel girder near the loading section yielded in tension, and the ultimate tensile strain was more than 10,000 $\mu\varepsilon$, which indicated that the plasticity was fully developed. When the load reached 340 kN (about 11.3 times of the design load and about 0.85 Pu), the web of the steel girder near the loading section also yielded and gradually entered into the tension state and yielded from bottom to top. However, the top flange of the steel girder did not enter into the plastic state. It showed that the neutral axis was always under the top flange, and there remained an elastic core near the neutral axis.

(3) Strain on the Steel Crossbeams. The steel beam and bridge deck are important components to connect and ensure the overall mechanical performance of the steel beam, and the maximum deflection difference of the internal and external steel beams occurs in the loading section. Therefore, two strain gauges are arranged at the upper and lower edges of the two ends of the small beam at the loading section to measure the stress state of the beam during the whole loading process. Figure 10 shows the load-strain curve (with tensile strain as positive) of the steel crossbeam near the loading section. It is found that the stress level of the steel beam is very low, until failure.

3.2.3. Strain on the Concrete Slab

(1) Strain of the Concrete Slab in the Hogging Moment Region. According to the Chinese concrete structure design code (GB50010-2002) [36], the splitting tensile strength of concrete was 3.34 MPa, and the corresponding strain was 125 $\mu\varepsilon$, where microcracks began to appear in the concrete. Actually, the strain had been slightly larger than 125 $\mu\varepsilon$ when the crack was observed through naked eyes. The corresponding concrete tensile strain was close to 160 $\mu\varepsilon$. After that, strain gauges failed with the concrete cracking, so it was considered that there was no practical significance when the value of the strain gauge was over large. Figure 11 shows the relationships between load and concrete strain at the intermediate support section.

In Figure 11(a), it was found that the strain increased linearly up to the crack initiation as the load increased. After the first crack initiated, the tensile strains increased rapidly. When strains reached 100 $\mu\varepsilon$, the corresponding load value was about 40 kN (about 1.3 times of the design load and about 0.1 Pu). When the load was up to 60 kN (2 times of the design load and about 0.15 Pu), the corresponding strain value reached around 160 $\mu\varepsilon$. At this time, cracks initiated at

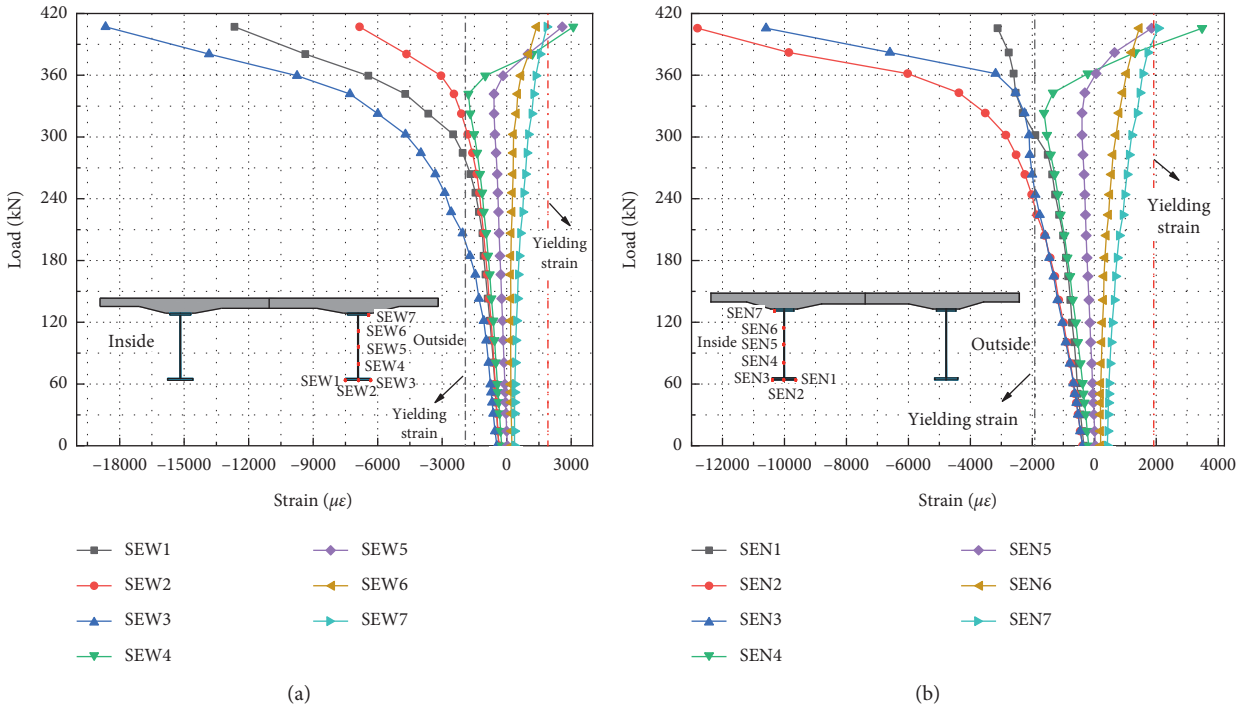

Figure 8: Load-strain curves of steel main girders at the intermediate support section (a) on the external steel main girder and (b) on the internal steel main girder.

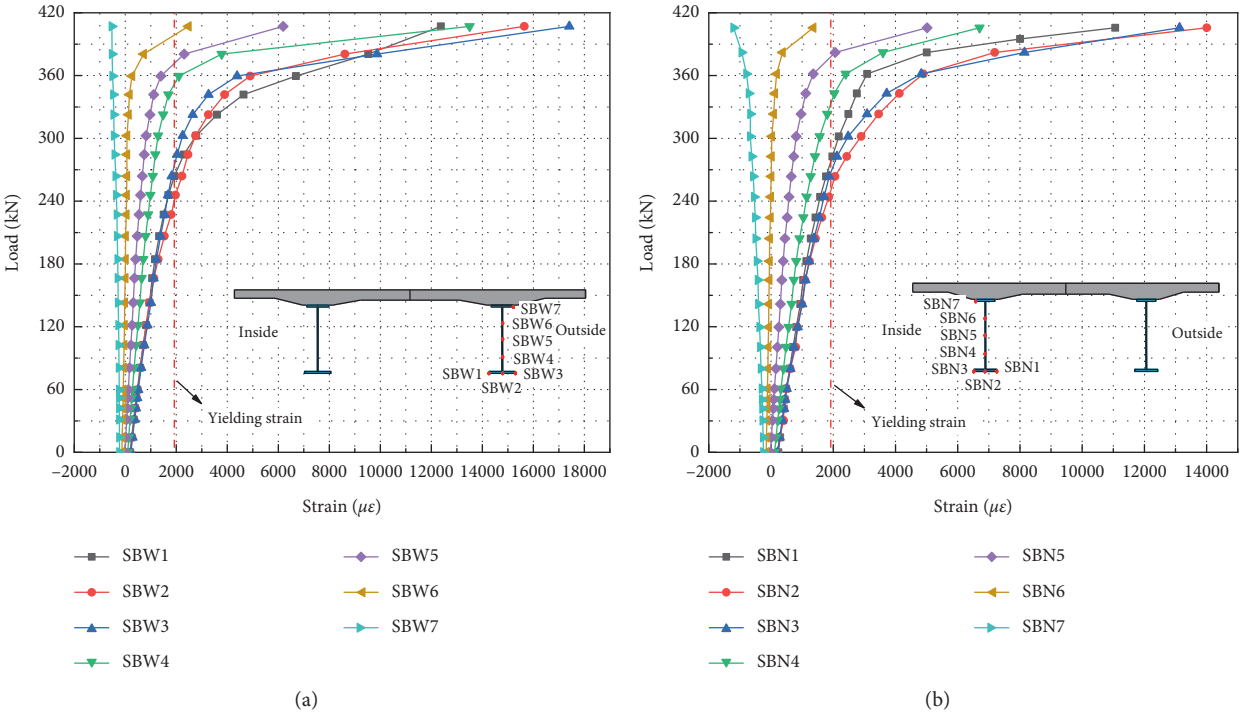

Figure 9: Load-strain curves of steel main girders at the loading section (a) on the external steel main girder and (b) on the internal steel main girder.

the top surface of the concrete slab. The last load level in case of cracks was defined as the cracking load of the concrete slab [37]. So, the cracking load was taken as about 50 kN (about 1.7 times of the design load and about 0.12 Pu). Based on Figure 11(a), it may also be noticed that the longitudinal strain is nonuniform in transverse distributions, and

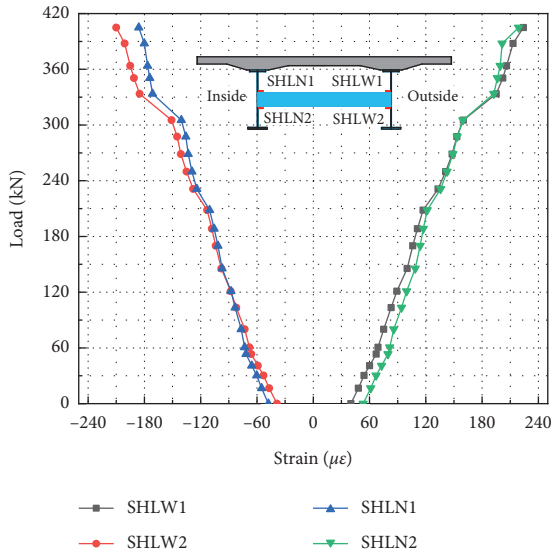

Figure 10: Load-strain curves of the steel crossbeam at the loading section.

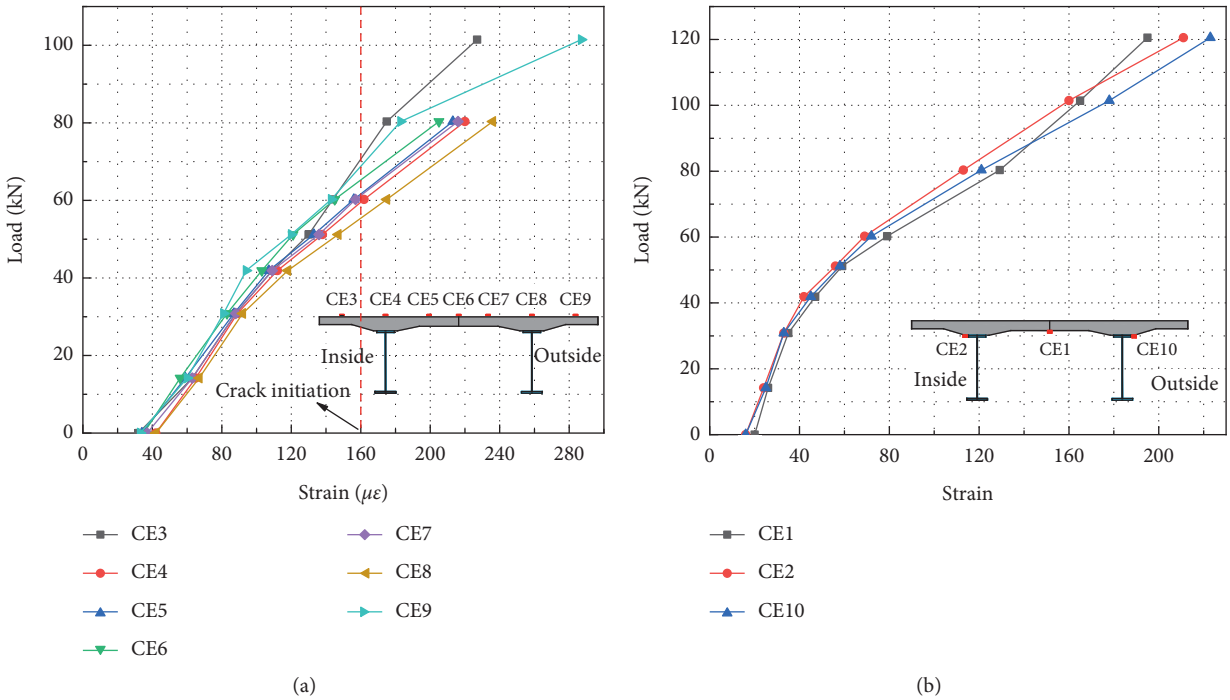

Figure 11: Load-strain relationship on the concrete slab at the intermediate support section (section *E*). (a) Top surface of the concrete slab. (b) Bottom surface of the concrete slab.

longitudinal strain reached its maximum at the web-flange junction and decreased away from it. When the load was lower, the shear lag effect was not obvious because the stress was small, and the full section was elastic. As the load increased, the concrete slab began to crack around the web-flange junction and was extended to both sides, and the shear lag effect became more pronounced. In Figure 11(b), it was found that the strain values of the three measuring points at the bottom surface were close at the beginning, but with the increase of load, the strain values at the outer side of the curve were larger than those at the inner side. When the load was close to 80 kN (about 2.7 times of the design load and about 0.2 Pu), the microcrack began to appear on the lower edge concrete, and the strain increased rapidly, indicating that the crack had penetrated the full concrete section. It also means that the composite section near the intermediate support section transformed into a cracked section.

(2) Strain of the Concrete Slab at the Positive Moment Region. Figure 12 shows the relationships between the load and concrete strain at the loading section (section *B* in Figure 5(a)). In Figure 12(a), it was clearly found that the

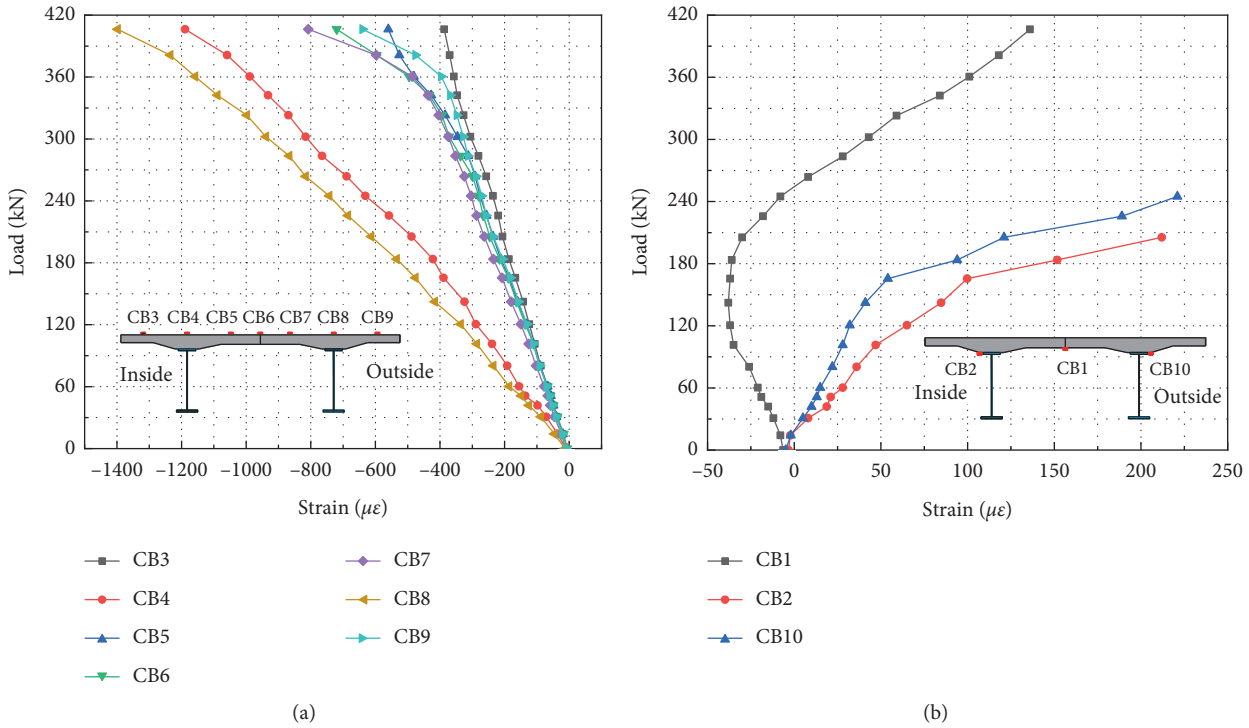

Figure 12: Load-strain relationship on the concrete slab at the loading section (section *B*). (a) Top surface of the concrete slab. (b) Bottom surface of the concrete slab.

strain at the top surface of the concrete slab increased linearly as the load increased at the beginning. When the load increased up to 360 kN (about 12 times of the design load and about 0.88 Pu), the slope of the load-strain curves decreased, and the strains increased rapidly. It indicated that the stiffness of the bridge mode decreased. However, the transverse crack on the upper surface of concrete due to the crushing of the concrete was located directly below the steel plate and did not pass through the strain gauge. So, in Figure 12(a), the strain measured by the strain gauge did not reach the crushing strain (3000 $\mu\varepsilon$). It is worth noting that the shear lag effect at the loading section was more pronounced than that at the intermediate support section. In the process of loading, with the neutral axis moving upward gradually, the bottom surface of the concrete slab gradually changed from compression to tension, and the tensile strain near the web-flange junction developed rapidly. Finally, all of them exceeded the splitting tensile strength and cracked, as shown in Figure 12(b).

3.2.4. Cross-Section Strain Distribution. Take a loading section (section *B*) as an example, the distribution of the longitudinal normal strain increment along the height of the composite girder at different load steps is shown in Figure 13. At the early loading stage ($\varepsilon < \varepsilon_y$), the strain increment points were linearly distributed along the height of the composite girder, satisfying the assumption of the plane section. When the strain exceeds the yielding strain ε_y, the points can no longer be connected by a single

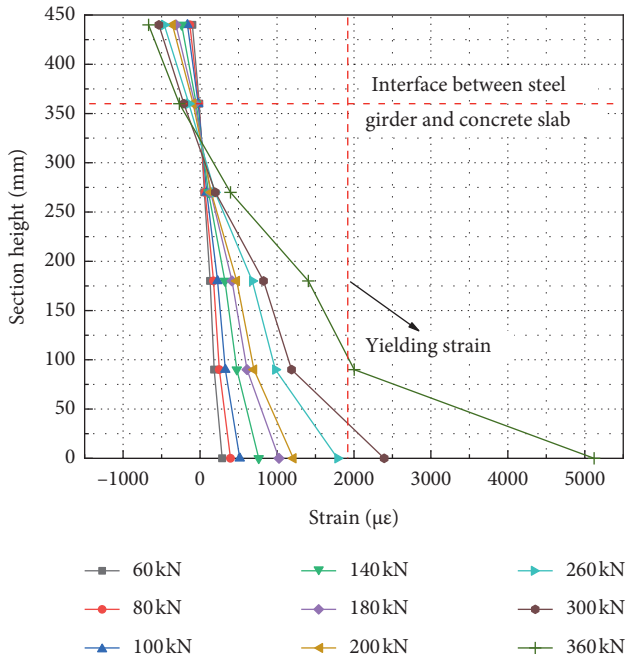

Figure 13: Strain distribution along the height of the section at the loading section (section *B*).

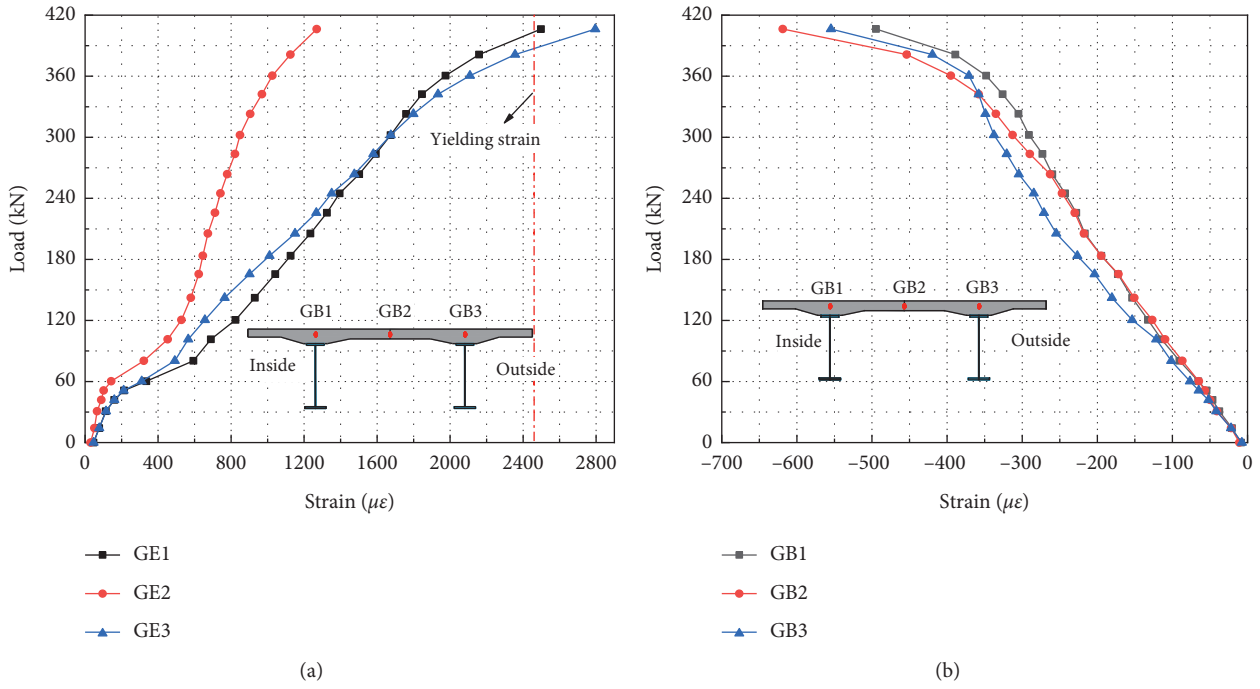

Figure 14: Load-strain curves of longitudinal reinforcement. (a) At the intermediate support section. (b) At the loading section.

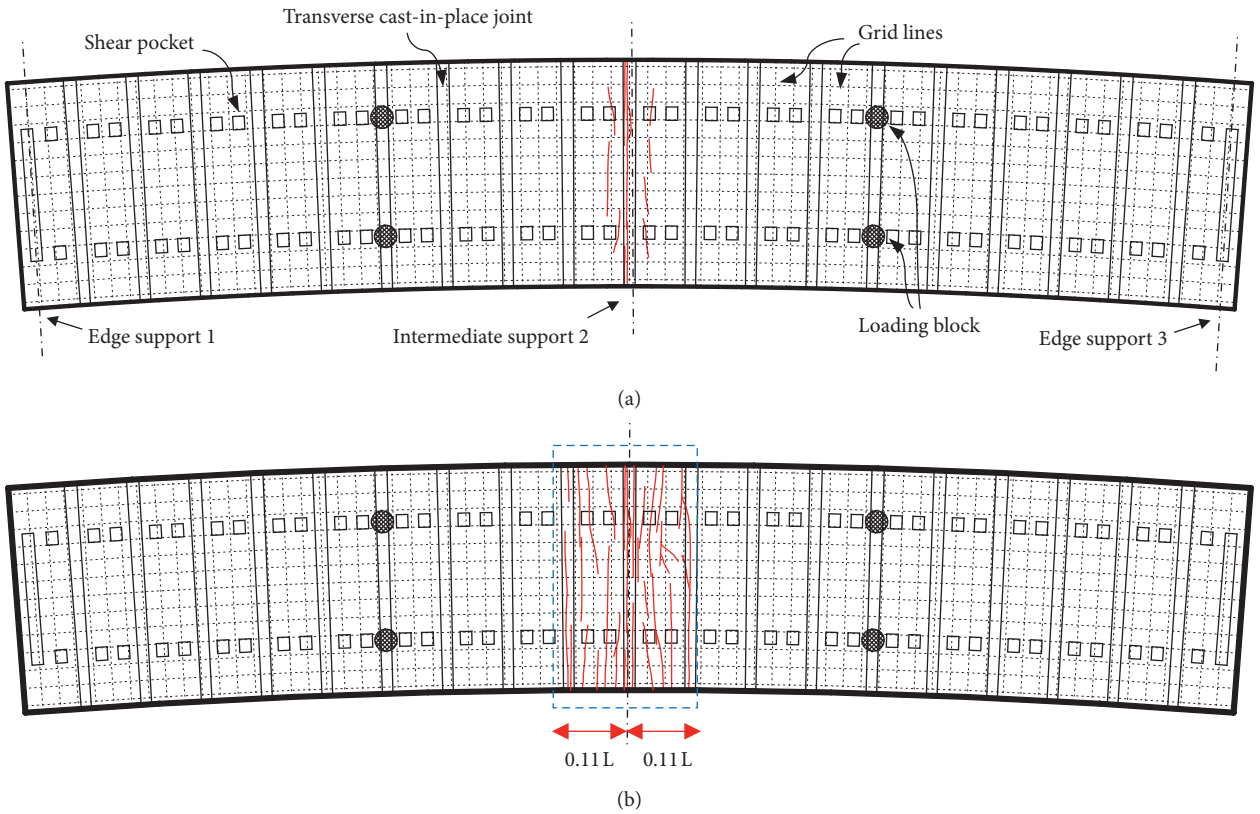

Figure 15: Schematic diagram of the concrete slab cracking process and distribution. (a) Cracking distribution under 140 kN loading force. (b) Cracking distribution under ultimate failure.

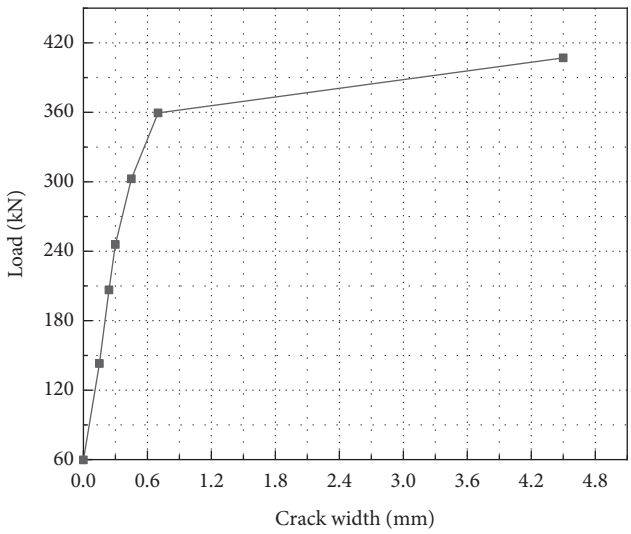

Figure 16: Load-crack width curve of the major crack.

straight line. It means the assumption of the plane section can no longer be valid. In addition, with the increase of loads, the bottom flange and web of the steel beam yielded gradually, and the neutral axis tended to move upward.

3.2.5. Strain of Longitudinal Reinforcement. Figure 14 shows the relationships between the load and the longitudinal reinforcement strain at the intermediate support section and the loading section, respectively. According to the results of the material property test, the yielding strain of longitudinal reinforcement was 2460 $\mu\varepsilon$. As shown in Figure 14(a), the strain of reinforcement increased linearly with the increase of load in the initial loading stage (up to 50~60 kN). And then, the increase rate of longitudinal reinforcement strain increased suddenly, which was attributed to the gradual cracking of concrete. With the increase of crack width, the concrete at a crack lost tensile strength gradually, and the applied load was transferred to the longitudinal reinforcement. From then on, the longitudinal reinforcement strain increased steadily until longitudinal reinforcement yielding. The yielding load of the longitudinal reinforcement was about 390 kN.

It could be seen from Figure 14 that when the ultimate failure state was reached, the longitudinal reinforcement in the hogging moment region had reached yield, while the longitudinal reinforcement at the loading section was far less than the yield strength, as shown in Figure 14(b). When we calculated the flexural capacity according to the current China highway standard specifications (Specifications for Design and Construction of Highway Steel-Concrete Composite Bridge) [34], we considered the mechanical resistance of longitudinal rebars in the hogging zone, while we neglected the mechanical resistance of longitudinal rebars in the sagging zone. The test results showed that this method was reasonable.

3.2.6. Concrete Slab Cracking Distribution and Crack Width. The schematic diagram of the concrete slab cracking process and distribution is shown in Figure 15. When the load was about 60 kN, the first transverse crack (initial transverse crack) was detected through the naked eye at the edge of the transverse cast-in-place joint over the intermediate support, where the construction joint surfaces had weak points of cracking because of the different concrete age between precast slabs and cast-in-place joints. Thus, before casting in the transverse joints, the surfaces should be cleaned and be made rough using a water jet to increase bonding.

With the load increased gradually, the first crack became a major crack. It extended gradually from the outer flange of the concrete slab to the inner along the transverse direction of the bridge. Meanwhile, a few cracks also occurred at the shear pockets in the precast slab on both sides of the main crack. When the load is 140 kN (about 4.7 times of the design load and about 0.34 Pu), the major crack runs through the slab transverse direction, which causes the concrete of the intermediate support section to step out of work gradually. At that time, the width of the major crack was 0.15 mm, and twelve cracks had been observed on the concrete slab in the hogging moment region. From 140 kN to 360 kN, microcracks appeared and extended gradually. And when the load reached 200 kN (about 6.7 times of the design load and about 0.5 Pu), the width of the major crack was 0.25 mm. When the load reached about 360 kN (about 12 times of the design load and about 0.88 Pu), there had been about 20 transverse cracks in the negative moment region. The width of the major cracks was 0.35 mm. The cracks at the cast-in-place joints developed to 0.25 mm wide, and the other visible cracks were basically more than 0.1 mm wide. From then on, the number of cracks in the hogging moment region was not increased any more. When the load was close to 407 kN (Pu), both the width of the existing cracks and the deflection at the loading point increased rapidly. The stiffness of the intact continuous composite bridge model decreased drastically.

Finally, an obvious angle appeared at the intermediate support section, as shown in Figure 6. The major crack reached 4.5 mm wide. At that time, cracks propagated throughout the two precast slabs and cast-in-place joints on both sides of the intermediate support section. That is to say, the composite section within a range of ±11% L from the intermediate support had become the cracked section. It is also indicated that it is reasonable and safe to presume the area within 15% of the span on both sides of the bearing in the negative moment as the cracking area in Eurocode 4.

The load-crack width of the major crack curve is presented in Figure 16. The width of the major crack grew linearly approximately before the longitudinal reinforcement yielded at the intermediate support section. Once the longitudinal reinforcement yielded and the plastic hinge was formed on the intermediate support section, the width of the major crack increased sharply. In addition, the load-crack width curve could also show the limitation of service load for crack control in composite girders with precast slabs. We can see from Figure 16 that when the major crack is 0.2 mm wide, the load is 150 kN (about 5 times of the design load).

4. Conclusions

By a comprehensive and cautious static test on the 1/5-scale bridge model, mechanical behavior, ultimate load carrying capacity, and failure modes were investigated. Moreover, crack development and major crack width at the top surface of the concrete slab in the hogging moment region were also reported and measured. Based on the experimental test and analysis, the main results of this test were concluded as follows:

(1) The failure mode of the curved bridge model under four monotonic symmetric concentrated forces near the midspan position was obtained. Concrete slabs cracked within the range of ±11% of the span from the intermediate support. The concrete slabs were crushed at the top of the concrete slab near the loading position. The longitudinal reinforcement yielded in the hogging moment region. The webs of the main girders were buckled locally at the loading position and intermediate support section, respectively. Finally, the whole bridge model was deformed to an obvious "*W*" shape (Figure 6). In accordance with Eurocode 4, the sectional classes in hogging moment regions for the bridge model were regarded as class 2.

(2) The load-deflection curves of the internal and external girders had similar changing law, which could be divided into three stages: elastic stage, elastic-plastic stage, and failure stage. There were slight differences between the stiffness of the internal girder and that of the external girder. The rigidity of the external girder was less than that of the internal girder. However, the ultimate bearing capacity was basically the same. The composite girder had high ductility. And the ductility of the external main girder was higher than that of the internal main girder. The displacement ductility coefficients of the internal and external girders were 4.06 and 4.40, respectively.

(3) Based on the similarity principle, in the bridge model, as well as the prototype bridge, the cracking load was about 1.7 times of the design load. When the major crack was 0.2 mm wide, the load was about 5 times of the design load. The yield load was about 6.3 times of the design load, as well as half of the ultimate load. The ultimate load was about 13.6 times of the design load. These may indicate that the twin I-girder composite bridge designed by the current China highway standard specifications had a high safety reserve.

(4) The first crack was detected through the naked eye at the edge of the transverse cast-in-place joint over the intermediate support. It indicated that construction joint surfaces are weak points of cracking of this type of fabricated bridge deck. Thus, before casting in the transverse joints, the surfaces should be cleaned and be made rough to increase bonding. Moreover, the cracks occurred within the range of ±11% of the span from the intermediate support. It is indicated that it is reasonable and safe to presume the area within 15% of the span on both sides of the bearing in the negative moment as the cracking area. The shear lag effect was more pronounced after crack occurred than that before crack occurred.

Data Availability

The data used to support the findings of this study are included within the article.

Conflicts of Interest

The authors declare that they have no conflicts of interest.

Acknowledgments

This study was supported by Shanxi Transportation Technology Project (no. 18-14K) and the Shanxi National Science Foundation (no. 2020JQ-377). The financial support is gratefully appreciated. The assistance for experimental studies from China Shanxi Expressway Construction Group Company, Chang'an University, China Railway Baoqiao Group Co., Ltd., and China Railway 18th Bureau Group Co., Ltd. is also appreciated.

References

[1] M. P. Culmo, *Accelerated Bridge Construction-Experience in Design: Fabrication and Erection of Prefabricated Bridge Elements and Systems*, Federal Highway Administration, Washington, DC, USA, 2011.

[2] H.-K. Ryu, S.-P. Chang, Y.-J. Kim, and B.-S. Kim, "Crack control of a steel and concrete composite plate girder with prefabricated slabs under hogging moments," *Engineering Structures*, vol. 27, no. 11, pp. 1613–1624, 2005.

[3] D. Fa-Xing, L. Jing, L. Y. Xue-Mei, and L. Yong-Suo, "Experimental investigation on hysteretic behavior of simply supported steel-concrete composite beam," *Journal of Constructional Steel Research*, vol. 144, pp. 153–165, 2018.

[4] D. Zhi-Wu, J. V. Marti, and V. Yepes, "Steel-concrete composite bridges: design, life cycle assessment, maintenance, and decision-making," *Advances In Civil Engineering*, vol. 2020, p. 13, 2020.

[5] R. Wodzinowski, K. Sennah, and H. M. Afefy, "Free vibration analysis of horizontally curved composite concrete-steel I-girder bridges," *Journal of Constructional Steel Research*, vol. 140, pp. 47–61, 2018.

[6] C. Machelski and R. Toczkiewicz, "Effects of connection flexibility in steel-concrete composite beams due to live loads," *Archives of Civil and Mechanical Engineering*, vol. 6, no. 1, pp. 65–86, 2006.

[7] Federal Highway Adminstration, *Accelerated Bridge Construction Manual*, Federal Highway Adminstration, Washington, DC, USA, 2011.

[8] M. A. Khan, *Accelerated Bridge Construction*, Butter Worth-Heinemann, Oxford, UK, 2014.

[9] Y. Zhao and Z. Yi, "Effects of Initial stress on the in-plane ultimate bearing capacity of CFST arch bridges," *Journal of Hunan University*, vol. 34, pp. 1–5, 2007.

[10] J. B. Kennedy and M. Soliman, "Ultimate loads of continuous composite bridges," *Journal of Structural Engineering*, vol. 118, no. 9, pp. 2610–2623, 1992.
[11] Z. Liu, "Study on model test of bridge structure," *Bridge Construction*, vol. 4, pp. 1–7, 1999.
[12] S. Jeon, J. Kim, Y. Seo, and C Hong, "Effect of a fault and weak plane on the stability of a tunnel in rock-a scaled model test and numerical analysis," *International Journal of Rock Mechanics and Mining Sciences*, vol. 41, no. 3, pp. 658–663, 2004.
[13] B. Wu and L. U. Wen-long, "Model test of RC frame-shear wall structure with partial columns sliding at upper ends," *Engineering Mechanics*, vol. 2, pp. 163–170, 2015.
[14] T. H. T. Chan and D. B. Ashebo, "Moving axle load from multi-span continuous bridge: laboratory study," *Journal of Vibration and Acoustics*, vol. 128, no. 4, pp. 521–526, 2006.
[15] C. S. Shim and S. P. Chang, "Cracking of continuous composite beams with precast decks," *Journal of Constructional Steel Research*, vol. 59, no. 20, pp. 1–14, 2003.
[16] H.-K. Ryu, C.-S. Shim, S.-P. Chang, and C.-H. Chung, "Inelastic behaviour of externally prestressed continuous composite box-girder bridge with prefabricated slabs," *Journal of Constructional Steel Research*, vol. 60, no. 7, pp. 989–1005, 2004.
[17] H.-K. Ryu and S.-P. Chang, "Ultimate strength of continuous composite box-girder bridges with precast decks," *Journal of Constructional Steel Research*, vol. 61, no. 3, pp. 329–343, 2005.
[18] A. Androus, H. M. Afefy, and K. Sennah, "Investigation of free vibration and ultimate behavior of composite twin-box girder bridges," *Journal of Constructional Steel Research*, vol. 130, pp. 177–192, 2017.
[19] W. Lin, T. Yoda, and T. Yoda, "Experimental and numerical study on mechanical behavior of composite girders under hogging moment," *Advanced Steel Construction*, vol. 9, no. 4, pp. 309–333, 2013.
[20] W. Lin, T. Yoda, and N. Taniguchi, "Fatigue tests on straight steel-concrete composite beams subjected to hogging moment," *Journal of Constructional Steel Research*, vol. 80, pp. 42–56, 2013.
[21] W. Lin, T. Yoda, Y. Kumagai, and T. Saigyo, "Numerical study on post-fracture redundancy of the two-girder steel-concrete composite highway bridges," *International Journal of Steel Structures*, vol. 13, no. 4, pp. 671–681, 2013.
[22] J. He, Y. Liu, A. Chen, and T. Yoda, "Experimental study on inelastic mechanical behaviour of composite girders under hogging moment," *Journal of Constructional Steel Research*, vol. 66, no. 1, pp. 37–52, 2010.
[23] W. Lin and T. Yoda, "Numerical study on horizontally curved steel-concrete composite beams subjected to hogging moment," *International Journal of Steel Structures*, vol. 14, no. 3, pp. 557–569, 2014.
[24] D. B. Kim and B. J. Choi, "Evaluation of flexural strength about shape of the steel plate-concrete composite beam with bolt," *Advanced Materials Research*, vol. 1021, pp. 144–147, 2014.
[25] Y.-H. Wang, J. Yu, J.-P. Liu et al., "Experimental study on assembled monolithic steel-prestressed concrete composite beam in negative moment," *Journal of Constructional Steel Research*, vol. 167, pp. 143–164, 2020.
[26] J. B. Kennedy and N. F. Grace, "Load distribution in continuous composite bridges," *Canadian Journal of Civil Engineering*, vol. 10, no. 3, pp. 384–395, 1983.
[27] M. Soliman and J. B. Kennedy, "Load distribution in composite bridges at the ultimate limit state," in *Proceedings of the Third International Conference on Short and Medium Span Bridges*, pp. 201–214, Toronto, Canada, 1990.
[28] H.-K. Ryu, Y.-J. Kim, and S.-P. Chang, "Crack control of a continuous composite two-girder bridge with prefabricated slabs under static and fatigue loads," *Engineering Structures*, vol. 29, no. 6, pp. 851–864, 2007.
[29] H.-H. Kim and C.-S. Shim, "Experimental investigation of double composite twin-girder railway bridges," *Journal of Constructional Steel Research*, vol. 65, no. 6, pp. 1355–1365, 2009.
[30] H. Lam and W. Lin, "Performance of composite twin i-girder bridges with fatigue-induced cracks," *Journal of Bridge Engineering*, vol. 22, no. 9, 2017.
[31] L. Han and G. Yao, "Effect of initial stress on bearing capacity of concrete-filled steel tubular beam-columns," *China Civil Engineering Journal*, vol. 4, pp. 9–18, 2003.
[32] China Architecture & Building Press, *Code for Design of Composite Structures (JGJ 138-2016)*, China Architecture & Building Press, Beijing, China, 2016.
[33] China Architecture & Building Press, *Code for Design of Steel Structures (GB50017-2017)*, China Architecture & Building Press, Beijing, China, 2017.
[34] People's Communications Press, *Specifications for Design and Construction of Highway Steel-Concrete Composite Bridge: JTG/T D64-01-2015)*, People's Communications Press, Beijing, China, 2015.
[35] BSI, *Design of Composite Steel and Concrete Structures, Part 2: Composite Bridges—DD ENV 1994-2*, BSI, London, UK, 1994.
[36] China Architecture & Building Press, *Code for Design of Concrete Structures (GB50010-2012)*, China Architecture & Building Press, Beijing, China, 2012.
[37] J. Jiang and X. Lu, *Finite Element Analysis of Concrete Structures*, Tsinghua University Press, Beijing, China, 2nd edition, 2013.